



Research Article

Analysis on Rheology of Unsteady Casson Fluid Flow through an Atherosclerotic Lesion

Chhama Awasthi^{*} , S. U. Siddiqui

Department of Mathematics, Harcourt Butler Technical University, Kanpur-208002, Uttar Pradesh, India
E-mail: awasthi.chhama@gmail.com

Received: 21 October 2022; **Revised:** 15 December 2022; **Accepted:** 4 January 2023

Abstract: In this study, the blood flow mechanism in an inclined artery with the unwanted growth inside the arterial wall has been investigated by modelling blood as a non-Newtonian Casson fluid. A significant quantitative investigation on various flow physical parameters, including axial velocity, volumetric flow rate, plug core radius, plug core velocity, wall shear stress, and effective viscosity, has been analyzed through numerical calculations under the assumption that blood flow is unsteady. According to this study, slip velocity, inclination, yield stress, stenosis height and Reynolds number all have made a considerable impact on flow characteristics during blood flow in the core region.

Keywords: stenosed artery, blood, pulsatile flow, casson fluid, plug core velocity, yield stress, effective viscosity

MSC: 76Z05, 92C10, 92C35

1. Introduction

Incomplete or complete artery occlusion is the cause of cardiovascular illnesses. Stenosis is defined by Rodbard [1] as an unfavorable development inside the artery's cavity. Acceleration causes our body to jerk, putting a lot of health issues at risk, including headaches, a raised pulse rate, etc. When blood circulates via microscopic vessels, it has a non-Newtonian nature [2, 3] in the core area and a Newtonian nature close to the arterial wall.

In a Casson fluid model, blood shows non-zero yield stress at low shear rates, in accordance with Casson's [4] observations. The Casson model was shown to be appropriate for blood flow via an artery with a 130-1,300 micrometre diameter by Merrill et al. [5]. Numerous studies, including Sankar and Lee, Chaturani and Ponnalagar Samy, Nagarani, and Sarojamma [6-9], have described the pulsatile Casson fluid flow via stenosed artery under the acceleration of the body.

All arteries in our body are not horizontal and vertical. Present study examines the blood flow through inclined stenosed blood artery. These circumstances are more likely to exist where the blood veins are curved, bifurcate, meet, have a side branch, or have an abrupt change in flow geometry and the flow is erratic. This will help in understanding the new insights of practical applications of physical phenomena of blood flow through inclined artery. Siddiqui & Awasthi [10] described the blood flow via stenosed artery having catheter inside it and observed the slip, unsteadiness and body acceleration. Sharma et al. [11] studied the effects of a magnetic field and body acceleration during blood flow

through an inclined artery. Srivastava et al. [12] worked on a non-Newtonian fluid flow model for the slip condition on blood flow through an inclined tapered stenosed artery using power-law fluid.

Dhange et al. [13] discussed blood flow via an inclined tube under the influence of magnetic field and a constant incompressible Casson fluid. Kumar et al. [14] discussed on comparative study of non-Newtonian physiological blood flow through elastic stenotic artery with rigid body stenotic artery. Sriyab [15] studied on the effect of stenotic geometry and non-Newtonian property of blood flow through arterial stenosis.

In a lid-driven square hollow filled with a porous material developed by Darcy Forchheimer, the effects of thermal radiation and heat generation on natural convection are explored in [16] and for non-Darcian natural convection is investigated by [17]. The two-dimensional laminar natural convection flow has been studied by [18]. Natural convection in a two-sided lid-driven inclined porous enclosure with a sinusoidal thermal boundary condition, is carried out by [19].

The effect of the aligned magnetic field on Williamson's nanofluid on a stretching surface with convective boundary conditions is investigated numerically in [20]. To investigate the effects of radiation, on the heat and mass transfer of magneto-Casson fluid over a vertical permeable plate by using FEM method has been observed in [21]. Tangent hyperbolic nanofluid flow over an electromagnetic surface with velocity slip and heat source are studied in [22]. The resolution of radiation effects on MHD micropolar fluid flow in the case of heat generation or absorption through a stretched porous surface is discussed in [23].

This mathematical model has been created to analyze the rheology of blood by examining various factors affecting the inclined blood flow as well as normal blood flow.

- It helps, to count the effects of Reynolds number, yield stress, non-Newtonian nature, stenosis height, and slip on an accelerating fluid in the artery in order to get adequate findings in this subject.

- Also, this study analyzes the blood flow in the core region of the artery under various rheological conditions. Blood flow remains steady when the artery's wall shear stress is lower than the yield stress, and it plugs when the yield stress is higher and equal to the wall shear stress.

- This model may be used in the future to explore alternative flow parameters for Newtonian fluid, and other non-Newtonian fluids over permeable wall. Also, we can observe the effects of magnetic field with nanoparticles on flow characteristics by using different numerical methods in the future.

2. Mathematical model

Let there be axially symmetric, laminar, unsteady, and fully developed blood flow in the stenosed artery. The Casson fluid is used to symbolize blood. The following section presents the mathematical impression for the radius of the artery (see Figure 1) that Sharma et al. [11] took into consideration.

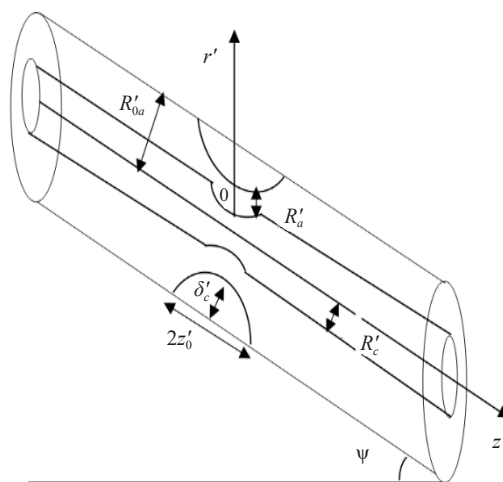


Figure 1. Geometry of stenosed artery in an inclined position

$$R'_a(z') = \begin{cases} R'_{0a} - \left(\frac{\delta'_c}{2}\right) \left\{1 + \cos\left(\frac{\pi z'}{z'_0}\right)\right\}, & \text{for } |z'| \leq z'_0, \\ R'_{0a}, & \text{for } |z'| > z'_0, \end{cases} \quad (1)$$

where δ'_c indicates maximum stenosis height, $R'_a(z')$ indicates the radius of the artery with a stenosis, R'_{0a} indicates the radius of the normal artery with a constant value, $2z'_0$ indicates the stenosis length, and $(\delta'_c/R'_{0a}) < 1$.

Equations (2) and (3), as used by Schlichting and Gersten [24], describe the momentum equations regulate the flow pattern.

$$\frac{\partial p'}{\partial r'} = 0 \quad (2)$$

$$\rho'_{Ca} \left\{ \left(\frac{\partial u'_c}{\partial t'} \right) - g_a \sin \psi' \right\} + \left(\frac{\partial p'}{\partial z'} \right) = B'_c(t') - \left(\frac{1}{r'} \right) \frac{\partial}{\partial r'} (r' \tau'_{wa}) \quad (3)$$

where u'_c denotes the axial velocity along the z' direction, p' denotes the pressure, t' denotes the time, ρ'_{ca} denotes the density, τ'_{wa} denotes the wall shear stress, ψ' denotes the inclination angle, g_a denotes the acceleration due to gravity and $B'_c(t')$ denotes the periodic body acceleration (equation 4) along the axial direction.

$$B'_c(t') = a_0 \cos(\phi + \omega'_{bc} t') \quad (4)$$

where ϕ and a_0 denotes the phase angle and amplitude of body acceleration with respect to the pressure gradient. Here $\omega'_{bc} = 2\pi f'_{bc}$; f'_{bc} denotes the frequency of body acceleration. Also, by taking f'_{bc} very small. The wave impact is not important.

Now the pressure gradient is

$$\frac{-\partial p'}{\partial z'}(z', t') = A_0 + A_1 \cos(t' \omega'_{pc}), \quad t' \geq 0 \quad (5)$$

The A_0 , pressure gradient in steady-state and the A_1 , amplitude of the fluctuating part are the functions of z' . Here ω'_{pc} indicates the frequency of oscillation of the pulsatile flow, and it's defined as $\omega'_{pc} = 2\pi f'_{pc}$, with f'_{pc} as the pulse rate frequency. Also, radial velocity can be neglected due to its small magnitude.

This equation (6), depicts how the Casson fluid functions,

$$\begin{cases} \sqrt{\tau'_{wa}} = \sqrt{\tau'_c} + \sqrt{\mu'_0 \left(-\frac{\partial u'_c}{\partial r'} \right)}; & \text{if } \tau'_{wa} \geq \tau'_c \\ \frac{\partial u'_c}{\partial r'} = 0, & \text{if } \tau'_{wa} < \tau'_c \end{cases} \quad (6)$$

where, τ'_c and μ'_0 denotes the yield stress, viscosity of Casson fluid respectively. In the core region ($\tau'_{wa} < \tau'_c$), the velocity gradient vanishes, and this shows the plug flow. However, fluid behavior is indicated in the region $\tau'_{wa} \geq \tau'_c$.

Considering the boundary conditions as

$$(i) \text{ At } r' = 0, \tau'_{wa} \text{ is finite} \quad (7)$$

$$(ii) \text{ At } r' = R'_a(z'), u'_c = u'_s \quad (8)$$

where u'_s denotes the axial slip velocity at the obstructed wall of the artery.

Now introducing the variables in the non-dimensional form as

$$\left. \begin{aligned} R_a(z) &= R'_a(z') / R'_{0a}, r = r' / R'_{0a}, d = d' / R'_{0a}, z = z' / R'_{0a}, \delta = \delta' / R'_{0a}, e = A_1 / A_0, \\ F &= A_0 / 4\rho'_{ca}g_a, t = t'\omega'_{pc}, \omega = \omega'_{bc} / \omega'_{pc}, B = a_0 / A_0, \tau_{wa} = \frac{\tau'_{wa}}{A_0R'_{0a}/2}, \tau_c = \frac{\tau'_c}{A_0R'_{0a}/2} \\ \alpha^2 &= \frac{R'_{0a}\omega'_{pc}\rho'_{ca}}{\mu'_0}, u_c = \frac{4u'_c\mu'_0}{A_0R'^2_{0a}}, u_s = \frac{4u'_s\mu'_0}{A_0R'^2_{0a}} \end{aligned} \right\} \quad (9)$$

where α denotes the pulsatile Reynolds number.

With the help of non-dimensional variables, equation (3) can be written as

$$\alpha^2 \left(\frac{\partial u_c}{\partial t} \right) = 4(e \cos t + 1) + 4B \cos(\phi + \omega t) - \left(\frac{2}{r} \right) \frac{\partial}{\partial r} (r\tau_{wa}) + \frac{\sin \psi}{F} \quad (10)$$

and equation (6) becomes

$$\left. \begin{aligned} \sqrt{\tau_{wa}} &= \sqrt{\tau_c} + \frac{1}{\sqrt{2}} \sqrt{\left(-\frac{\partial u_c}{\partial r} \right)}; \quad \text{if } \tau_{wa} \geq \tau_c \\ \frac{\partial u_c}{\partial r} &= 0, \quad \text{if } \tau_{wa} < \tau_c \end{aligned} \right\} \quad (11)$$

Now, the boundary conditions (7), (8) becomes

$$(i) \text{ At } r = 0, \tau_{wa} \text{ is finite} \quad (12)$$

$$(ii) \text{ At } r = R_a(z), u_c = u_s \quad (13)$$

The non-dimensional form of the radius of the artery, given in equation (1) becomes

$$R_a(z) = \begin{cases} 1 - \left(\frac{\delta_c}{2} \right) \left\{ 1 + \cos \left(\frac{\pi z}{z_0} \right) \right\}, & \text{for } |z| \leq z_0, \\ 1 & \text{for } |z| > z_0, \end{cases} \quad (14)$$

The volumetric flow rate in the non-dimensional form is defined below

$$Q(z, t) = 4 \int_0^{R_a(z)} u_c(z, r, t) r dr \quad (15)$$

where $Q(z, t) = \frac{Q'(z', t')}{\pi A_0 (R'_{0a})^4 / 8 \mu'_0}$; $Q'(z', t')$ denotes the volumetric flow rate.

Effective viscosity (μ'_e),

$$\mu'_e = \pi \left(-\frac{\partial p'}{\partial z'} \right) (R'_a(z'))^4 / Q'(z', t')$$

with the help of non-dimensional variables, it's defined as

$$\mu_e = R_a^4 (1 + e \cos t) / Q(z, t) \quad (16)$$

3. Analysis of the problem

The physical principle that stipulates that inertial effects are not relevant for smaller values of the frequency parameter that generates the pressure gradient is reflected in this paper's assumed form of the solution, which is obtained by utilizing the perturbation method. Due to the fact that non-dimensional equations (10), (11) have a time-dependent α^2 term, these equations should be expanded by α^2 . The axial velocity (u_c), wall shear stress (τ_{wa}), plug core radius (R_c), plug core velocity (u_p), and plug core shear stress (τ_p) in terms of α^2 (where $\alpha^2 \ll 0$) are as follows

$$u_c(z, r, t) = u_{0c}(z, r, t) + \alpha^2 u_{1c}(z, r, t) + \dots \quad (17)$$

$$\tau_{wa}(z, r, t) = \tau_{0wa}(z, r, t) + \alpha^2 \tau_{1wa}(z, r, t) + \dots \quad (18)$$

$$R_c(z, t) = R_{0c}(z, t) + \alpha^2 R_{1c}(z, t) + \dots \quad (19)$$

$$u_p(z, t) = u_{0p}(z, t) + \alpha^2 u_{1p}(z, t) + \dots \quad (20)$$

$$\tau_p(z, t) = \tau_{0p}(z, t) + \alpha^2 \tau_{1p}(z, t) + \dots \quad (21)$$

Substituting equations (17) and (18) in equation (10) and equating the α^2 terms and constant terms, we get

$$\frac{\partial}{\partial r} (r \tau_{0wa}) = 2r \left[(e \cos t + 1) + B \cos(\phi + \omega t) + \frac{\sin \psi}{4F} \right] \quad (22)$$

$$\frac{\partial u_{0c}}{\partial t} = -\frac{2}{r} \frac{\partial}{\partial r} (r \tau_{1wa}) \quad (23)$$

Integrating equation (22) between 0 and R_{0c} , and using boundary condition (12), we have

$$\tau_{0p} = R_{0c} D(t) \quad (24)$$

where $D(t) = \left[(e \cos t + 1) + B \cos(\phi + \omega t) + \frac{\sin \psi}{4F} \right]$.

Integrating equation (22) between R_{0c} and r and using equations (12) and (24), we get

$$\tau_{0wa} = r D(t) \quad (25)$$

Substituting equations (17) and (18) in equation (11), we get

$$-\frac{\partial u_{0c}}{\partial r} = 2 \left[\tau_{0wa} + \tau_c - 2\sqrt{\tau_{0wa}\tau_c} \right] \quad (26)$$

$$-\frac{\partial u_{1c}}{\partial r} = 2\tau_{1wa} \left[1 - \sqrt{\frac{\tau_c}{\tau_{0wa}}} \right] \quad (27)$$

Applying the expansion of u_c and τ_w from equation (17) and (18) in equation (12) and (13) we have,

$$(i) \text{ At } r = 0, \tau_{0wa}, \tau_{1wa} \text{ are finite} \quad (28)$$

$$(ii) \text{ At } r = R_a(z), u_{0c} = u_s, u_{1c} = 0 \quad (29)$$

Integrating equation (26) between r and R_a , and by using equations (25) and (29), we have

$$u_{0c} = u_s + D(t)R_a^2 \left[\frac{1 - (r/R_a)^2 - (8/3)\sqrt{a_1} \{1 - (r/R_a)^{3/2}\}}{+2a_1 \{1 - (r/R_a)\}} \right] \quad (30)$$

where $a_1 = \tau_c / D(t)R_a$.

From equation (30), the approximation u_{0p} of plug core velocity is

$$u_{0p} = u_s + D(t)R_a^2 \left[\frac{1 - (R_{0c}/R_a)^2 - (8/3)\sqrt{a_1} \{1 - (R_{0c}/R_a)^{3/2}\}}{+2a_1 \{1 - (R_{0c}/R_a)\}} \right] \quad (31)$$

Similarly solving equation (23) and using equations (30), (31) and boundary conditions (28), (29) we get the solutions for τ_{1wa}, τ_{1p} as

$$\tau_{1wa} = \left[\left\{ (\sqrt{a_1}R_a^2/3) - (R_a^2/4) \right\} r + (r^3/8) - (4/21)\sqrt{a_1}R_a^{1/2}r^{5/2} \right] D'(t) \quad (32)$$

$$\tau_{1p} = R_{0c} \left[\frac{\sqrt{a_1}R_a^{1/2}}{3D'(t)} (R_a^{3/2} - R_{0c}^{3/2}) - \left(\frac{1}{4} \right) (R_a^2 - R_{0c}^2) \right] D'(t) \quad (33)$$

From equations (25), (27), and (32), axial velocity u_{1c} is

$$u_{1c} = D'(t)R_a^4 \left[\frac{1}{4} \left(\frac{r}{R_a} \right)^2 - \frac{1}{16} \left(\frac{r}{R_a} \right)^4 + \sqrt{a_1} \left\{ \frac{53}{294} \left(\frac{r}{R_a} \right)^{7/2} - \frac{1}{3} \left(\frac{r}{R_a} \right)^{3/2} \right\} \right. \\ \left. + a_1 \left\{ \frac{4}{9} \left(\frac{r}{R_a} \right)^{3/2} - \frac{8}{63} \left(\frac{r}{R_a} \right)^3 - \frac{20}{63} \right\} - \frac{3}{16} \right] \quad (34)$$

From equation (34), u_{1p} expression of plug core velocity is

$$u_{1p} = D'(t)R_a^4 \left[\frac{1}{4} \left(\frac{R_{0p}}{R_a} \right)^2 - \frac{1}{16} \left(\frac{R_{0p}}{R_a} \right)^4 + \sqrt{a_1} \left\{ \frac{53}{294} \left(\frac{R_{0p}}{R_a} \right)^{7/2} - \frac{1}{3} \left(\frac{R_{0p}}{R_a} \right)^{3/2} \right\} - \frac{1}{3} \left(\frac{R_{0p}}{R_a} \right)^2 + \frac{143}{294} \right] + a_1 \left[\frac{4}{9} \left(\frac{R_{0p}}{R_a} \right)^{3/2} - \frac{8}{63} \left(\frac{R_{0p}}{R_a} \right)^3 - \frac{20}{63} \right] - \frac{3}{16} \quad (35)$$

With the help of equation (30), (31) and (34), (35) in (17) and (20), the axial velocity u_c ,

$$u_c = u_s + D(t)R_a^2 \left[1 - (r/R_a)^2 - (8/3)\sqrt{a_1} \left\{ 1 - (r/R_a)^{3/2} \right\} + 2a_1 \left\{ 1 - (r/R_a) \right\} \right] + \alpha^2 D'(t)R_a^4 \left[\frac{1}{4} \left(\frac{r}{R_a} \right)^2 \sqrt{a_1} \left\{ \frac{53}{294} \left(\frac{r}{R_a} \right)^{7/2} - \frac{1}{3} \left(\frac{r}{R_a} \right)^{3/2} - \frac{1}{3} \left(\frac{r}{R_a} \right)^2 + \frac{143}{294} \right\} + a_1 \left[\frac{4}{9} \left(\frac{r}{R_a} \right)^{3/2} - \frac{8}{63} \left(\frac{r}{R_a} \right)^3 - \frac{20}{63} \right] - \frac{3}{16} - \frac{1}{16} \left(\frac{r}{R_a} \right)^4 \right] \quad (36)$$

plug core velocity u_p can be obtained as

$$u_p = u_s + D(t)R_a^2 \left[1 - (R_{0c}/R_a)^2 - (8/3)\sqrt{a_1} \left\{ 1 - (R_{0c}/R_a)^{3/2} \right\} + 2a_1 \left\{ 1 - (R_{0c}/R_a) \right\} \right] + \alpha^2 D'(t)R_a^4 \left[\sqrt{a_1} \left\{ \frac{53}{294} \left(\frac{R_{0p}}{R_a} \right)^{7/2} - \frac{1}{3} \left(\frac{R_{0p}}{R_a} \right)^{3/2} - \frac{1}{3} \left(\frac{R_{0p}}{R_a} \right)^2 + \frac{143}{294} \right\} - \frac{3}{16} + a_1 \left[\frac{4}{9} \left(\frac{R_{0p}}{R_a} \right)^{3/2} - \frac{8}{63} \left(\frac{R_{0p}}{R_a} \right)^3 - \frac{20}{63} \right] + \frac{1}{4} \left(\frac{R_{0p}}{R_a} \right)^2 - \frac{1}{16} \left(\frac{R_{0p}}{R_a} \right)^4 \right] \quad (37)$$

Neglecting α^2 terms and higher powers of α terms from equation (19), and with the use of equation (24), the R_{0c} term of R_c can be obtained as

$$r|_{\tau_{op}=\tau_c} = R_{0c} = \frac{\tau_c}{D(t)} \quad (38)$$

Using equations (24), (25) and (32), (33) in equations (18) and (21), the wall shear stress τ_{wa} , τ_p can be expressed as

$$\tau_{wa} = \left(\tau_{owa} + \alpha^2 \tau_{1wa} \right)_{r=R_a} \quad (39)$$

$$\tau_p = \left(\tau_{op} + \alpha^2 \tau_{1p} \right)_{r=R_{0c}} \quad (40)$$

Using equation (15) and (36), the volumetric flow rate Q is

$$Q(z,t) = 4 \int_0^{R_a(z)} u_c(z,r,t) r dr$$

$$= Q_{z1} + Q_{z2} + Q_{z3} + Q_{z4} \quad (41)$$

where

$$Q_{z1} = 2R_{0c}^2 u_s + 2D(t)R_a^2 R_{0c}^2 \{1 - (R_{0c} / R_a)^2\}$$

$$- (16/3)R_a^2 R_{0c}^2 \sqrt{a_1} \{1 - (R_{0c} / R_a)^{3/2}\}$$

$$+ 4a_1 D(t)R_a^2 R_{0c}^2 \{1 - (R_{0c} / R_a)\}$$

$$Q_{z2} = 2R_a^2 u_s \{1 - (R_{0c} / R_a)^2\} + D(t)R_a^4 \left\{ \begin{array}{l} 1 - 2(R_{0c} / R_a)^2 \\ -(R_{0c} / R_a)^4 \end{array} \right\}$$

$$- D(t)R_a^4 \sqrt{a_1} \left\{ \begin{array}{l} (160/21) - (32/3)(R_{0c} / R_a)^2 \\ + (64/21)(R_{0c} / R_a)^{7/2} \end{array} \right\}$$

$$+ 4a_1 D(t)R_a^4 \{1 - (R_{0c} / R_a)^2\} - (8/3)a_1 D(t)R_a^3 \{1 - (R_{0c} / R_a)^3\}$$

$$Q_{z3} = 2\alpha^2 D'(t)R_a^4 R_{0c}^4 \{1 - (1/4)(R_{0c} / R_a)^2\} - (3/8)\alpha^2 D'(t)R_a^4 R_{0c}^2$$

$$+ \alpha^2 (1/147)D'(t)R_a^4 R_{0c}^2 \sqrt{a_1} \{143 + 53(R_{0c} / R_a)^{7/2}\}$$

$$+ \alpha^2 (8/9)D'(t)R_a^{5/2} R_{0c}^{7/2} a_1 \{1 - (2/7)(R_{0c} / R_a)^{3/2}\}$$

$$Q_{z4} = \alpha^2 D'(t)R_a^6 \left\{ \begin{array}{l} (3/8)(R_{0c} / R_a)^2 - (1/4)(R_{0c} / R_a)^4 \\ + (1/24)(R_{0c} / R_a)^6 - (1/6) \end{array} \right\}$$

$$+ \alpha^2 D'(t)R_a^6 \sqrt{a_1} \left\{ \begin{array}{l} (49/33) - (212/1617)(R_{0c} / R_a)^{11/2} \\ - (143/147)(R_{0c} / R_a)^2 \\ - (8/21)(R_{0c} / R_a)^{7/2} \end{array} \right\}$$

Neglecting higher powers of α terms and α^4 terms from the equation (19), the R_{1c} approximation of the plug core radius can be obtained as

$$R_{1c} = \frac{\tau_1(R_{0c})}{D(t)} \quad (42)$$

With the help of equations (19), (34), and (38), the R_c is

$$R_c = \frac{\tau_c}{D(t)} + \frac{\alpha^2 D'(t) R_{0c}}{D(t)} \left[\frac{\sqrt{a_1} R_a^{1/2}}{3D'(t)} (R_a^{3/2} - R_{0c}^{3/2}) - \left(\frac{1}{4}\right) (R_a^2 - R_{0c}^2) \right] \quad (43)$$

In dimensionless form, the effective viscosity is

$$\mu_e = (R_a(z))^4 (1 + e \cos t) / \{Q_{z1} + Q_{z2} + Q_{z3} + Q_{z4}\} \quad (44)$$

4. Numerical results and discussion

With the use of predefined parameters and MATLAB (R2022b), numerical computations of these quantities for their primary physiological importance have been carried out. The results of axial velocity (u_c), plug core velocity (u_p), plug core radius (R_c), flow rate (Q), wall shear stress (τ_{wa}) and effective viscosity (μ_e) are obtained and computed for the fixed values of $F = 0.2$, $n = 0.95$, $m = 2$, $\phi = 0.2$, $\tau_c = 0.1$, $\omega = 1$ [25-27]. Figure 2 depicts the variation of Reynolds number (α) on axial velocity (u_c) with axial distance (r) for different fixed parameters $F = 0.2$, $\phi = 0.2$, $e = 1$, $\omega = 1$, $t = 1$, $\delta_c = 0.1$, $u_s = 0.02$. It has been found that increase of pulsatile Reynolds number, enhances the axial velocity slightly from the previous place. Also, the periodicity in graph shows pulsatile nature of blood. This describes the normal pulsatile blood flow in human body.

Figure 3 depicts the influence of different parameters inclined angle (Ψ), slip velocity (u_s), wall shear stress (τ_c) and Reynolds number (α) on plug core velocity (u_p) versus axial distance (r) for $F = 0.2$, $\phi = 0.2$, $e = 1$, $\delta_c = 0.1$, $\omega = 1$, $t = 1$. It shows that an increase in Reynolds number, inclined angle, and slip velocity increases plug core velocity whereas decreases considerably when yield stress increases. This occurs as on increasing Reynolds number; flow becomes non-linear and maximum flow takes place and hence core velocity increases. Similarly slip velocity and inclined angle also enhances the plug core velocity due to more flow. In the core region, flow occurs when wall shear stress is more than the yield stress. Therefore, if yield stress is maximum, wall shear stress is also maximum and reduces the plug flow.

Figure 4 illustrates plug core velocity with time graph for different values of Body acceleration (B), and stenosis height (δ_c) with $F = 0.2$, $\phi = 0.2$, $\alpha = 0.2$, $\Psi = 30^\circ$, $e = 1$, $t = 1$, $\omega = 1$. Figure 4 describes that body acceleration enhances the plug core velocity while it decreases swiftly on increasing stenosis height with the increase of time from 0° to 120° and then it partially increases and decreases for time 120° to 180° and 180° to 240° respectively again it increases rapidly for 240° to 360° . On increasing body acceleration width of core region enhances and hence core velocity decreases.

Figure 5 sketches the graph of plug core radius (R_c), with axial distance (r) for distinct values of Reynolds number (α), body acceleration (B), stenosis height (δ_c), and yield stress (τ_c) with $F = 0.2$, $\phi = 0.2$, $e = 1$, $\omega = 1$, $u_s = 0.02$. Figure 5 depicted that plug core radius slightly increases on increasing the Reynolds number and yield stress while reduces for an increase in stenosis depth. Also, enhancement in body acceleration decreases the plug core radius. Figure 6 depicted the wall shear stress (τ_{wa}) variation with time (t) for distinct values of inclined angle (Ψ) and body acceleration (B) with $F = 0.2$, $\phi = 0.2$, $\omega = 1$. From Figure 6, it has been observed that the wall shear stress (τ_{wa}) diminishes as body acceleration (B) rises and fluctuated when time increases. It has symmetry and a minimum value at $t = 180^\circ$ whereas maximum at $t = 0^\circ$ and 360° . It occurs as blood is pulsatile in nature.

Effective viscosity (μ_e) versus body acceleration (B) is shown in Figure 7 for different values of slip velocity (u_s) and stenosis height (δ_c) with $F = 0.2$, $\phi = 0.2$, $\alpha = 0.5$, $B = 0$, $e = 0.05$, $\omega = 1$, $t = 1$. It has been noticed that increase in body acceleration and slip velocity reduces the viscosity due to more flow of blood inside the artery. whereas viscosity increases on increasing stenosis depth.

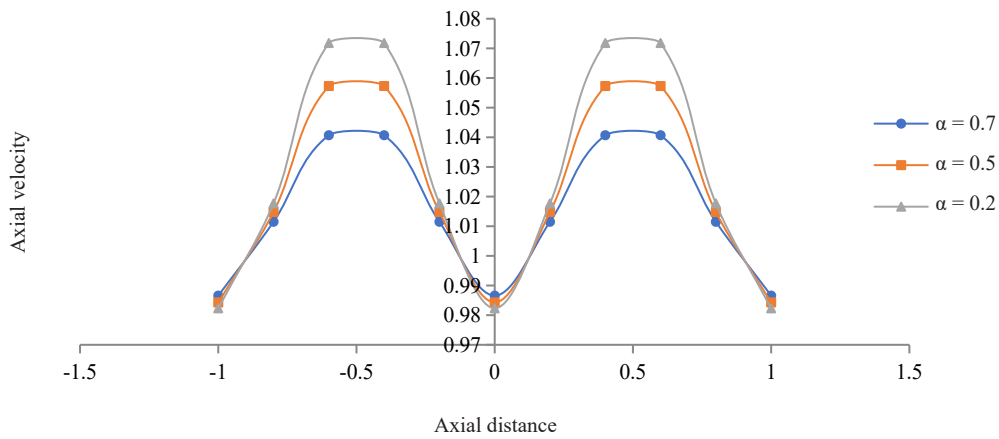


Figure 2. Variation of axial velocity with axial distance

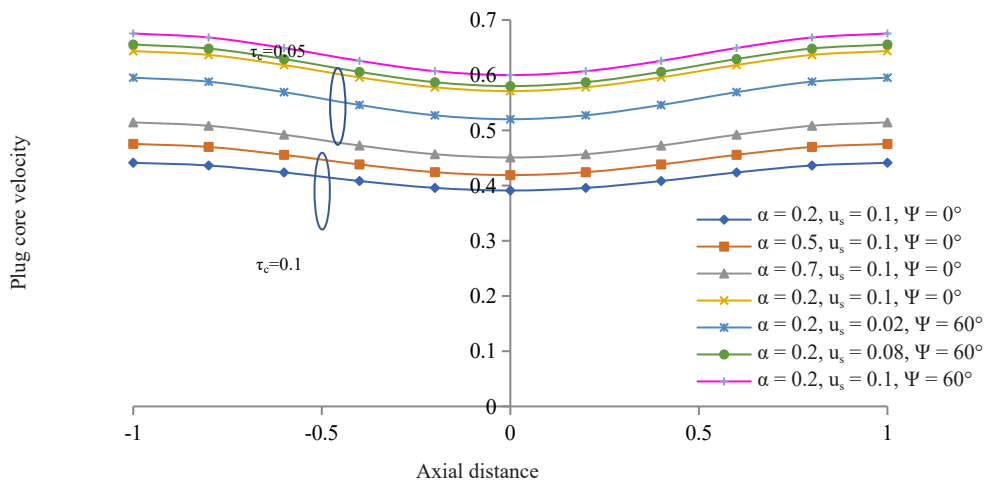


Figure 3. Variation of plug core velocity with axial distance

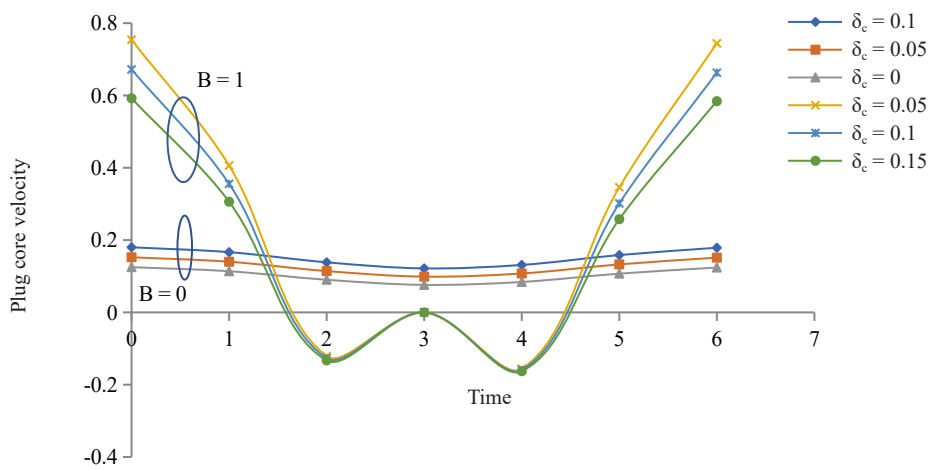


Figure 4. Variation of plug core velocity with time

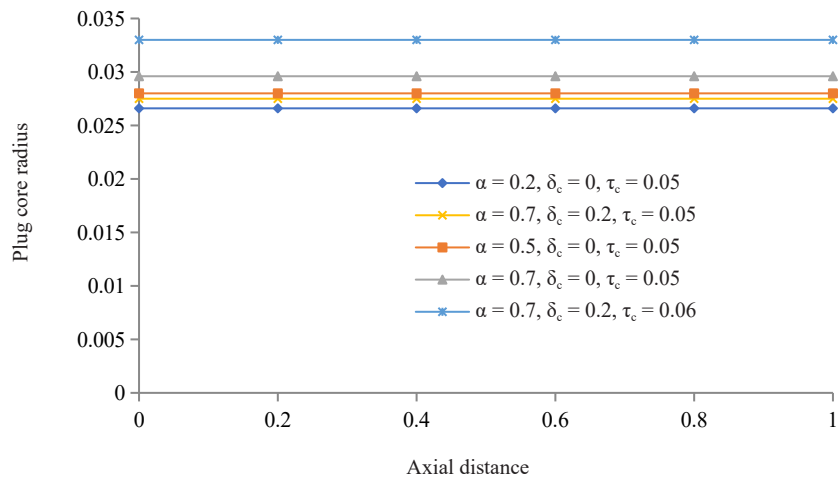


Figure 5. Variation of plug core radius with axial distance

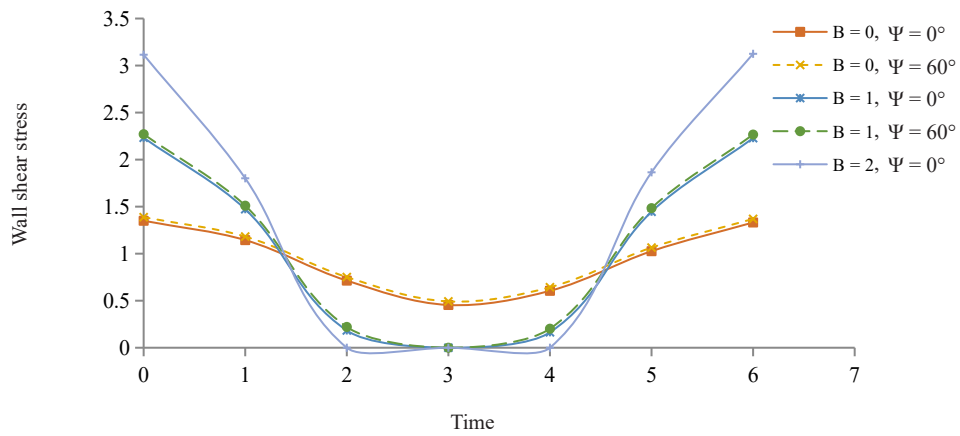


Figure 6. Variation of wall shear stress with time

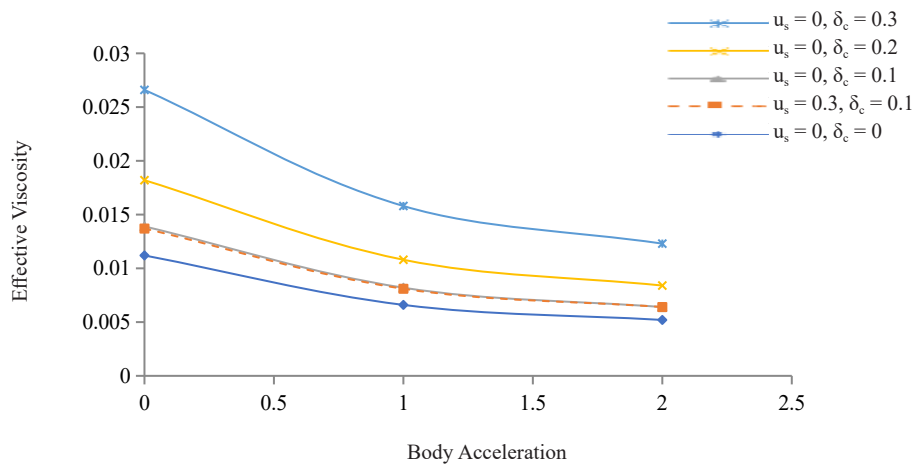


Figure 7. Variation of effective viscosity with body acceleration

5. Conclusions

Significant aspects of the rheology of pulsatile blood in an inclined stenosed artery have been examined in the current study and found that analytical results are in agreement with the experimental results. The major findings of the analysis are summarized as follows:

- Raising the Reynolds number, the axial velocity increases and the formation of periodic pattern exhibits the pulsatility of blood flow.
- Plug core velocity decreases as yield stress and stenosis height increases while it increases as Reynolds number, inclined angle, slip velocity, and body acceleration increases and shows symmetry in graph.
- Plug core radius increases for greater yield stress and Reynolds number.
- Wall shear stress diminishes as body acceleration rises and fluctuated over the time.
- Viscosity increases with increasing stenosis depth and decreases as body acceleration and slip velocity increase.

Another conclusion that could be drawn is that slip could aid to lessen damage to the vessel wall. Therefore, this research may aid doctors in determining the extent of stenosis and its long-term effects or in the treatment of cardiovascular ailments including myocardial infarction, stroke, heart attacks, etc. In the event of more severe stenosis, this investigation may be furthered by the addition of other rheological and physical data.

Funding statement

This research did not receive any specific grant from funding agencies in the public, commercial, or not-for-profit sectors.

Conflicts of interest

The authors declare that there are no conflicts of interest regarding the publication of this paper.

References

- [1] Rodbard S. Dynamics of blood flow in stenotic vascular lesion. *American Heart Journal*. 1966; 72: 698-704.
- [2] Bugliarello G, Sevilla J. Velocity distribution and other characteristics of steady and pulsatile blood flow in fine glass tubes. *Biorheology*. 1970; 7: 85-107.
- [3] Sankar DS, Lee U. Mathematical modeling of pulsatile flow of non-Newtonian fluid in stenosed arteries. *Communication in Nonlinear Sciences and Numerical Simulation*. 2009; 14: 2971-2981.
- [4] Casson N. A flow equation for pigment oil suspensions of printing ink type. In Mill, C. C. (ed.) *Rheology of Dispersed System*. London: Pergamon Press; 1959.
- [5] Merrill EW, Benis AM, Gilliland ER, Sherwood TK, Salzman EW. Pressure flow relations of human blood in hollow fibers at low shear rates. *Journal of Applied Physics*. 1965; 20: 954-967.
- [6] Chaturani P, Ponnalagar Samy R. Pulsatile flow of a Casson fluid through stenosed arteries with application to blood flow. *Biorheology*. 1986; 23: 499-511.
- [7] Nagarani P, Sarojamma G. Flow of a Casson fluid through a stenosed artery subject to periodic body acceleration. *Proceedings of the 9th WSEAS International Conference on Mathematical and Computational Methods in Science and Engineering*. Trinidad and Tobago; 2007. p. 5-7.
- [8] Nagarani P, Sarojamma G. Effect of body acceleration on a pulsatile flow of Casson fluid through a mild stenosed artery. *Korea-Australia Rheology*. 2008; 20(4): 189-196.
- [9] Sankar DS, Lee U. Nonlinear mathematical analysis for blood flow in a constricted artery under periodic body acceleration. *Communications in Nonlinear Science and numerical Simulation*. 2011; 16(11): 4390-4402.
- [10] Siddiqui SU, Awasthi C. Mathematical modelling of pulsatile herschel bulkley fluid flow through an inclined stenosed artery. *International Journal of Mathematical Archive*. 2017; 8(7): 205-215.
- [11] Sharma MK, Singh K, Bansal S. Pulsatile MHD flow in an inclined catheterized stenosed artery with slip on the

wall. *Journal of Biomedical Science and Engineering*. 2014; 7: 194-207.

- [12] Srivastava N. The Casson fluid model for blood flow through an inclined tapered artery of an accelerated body in the presence of magnetic field. *International Journal of Biomedical Engineering and Technology*. 2014; 15(3): 198-210.
- [13] Schlichting H, Gersten K. *Boundary Layer Theory*. Springer-Verlag; 2004.
- [14] Dhange M, Sankad G, Safdar R, Jamshed W, Eid MR, Bhujakkanavar U, et al. A mathematical model of blood flow in a stenosed artery with post-stenotic dilatation and a forced field. *PLOS ONE*. 2022; 17(7): e0266727. Available from: doi: 10.1371/journal.pone.0266727.
- [15] Kumar S, Kumar S, Kumar D. Comparative study of non-Newtonian physiological blood flow through elastic stenotic artery with rigid body stenotic artery. *Series on Biomechanics*. 2020; 34(4): 26-41.
- [16] Sriyab S. The effect of stenotic geometry and non-Newtonian property of blood flow through arterial stenosis. *Cardiovascular & Hematological Disorders-Drug Targets*. 2020; 20: 16-30.
- [17] Young DF, Tsai FY. Flow characteristics in models of arterial stenosis - I. Steady flow. *Journal of Biomechanics*. 1973; 6: 395-411.
- [18] Liepsch DW. Flow in tubes and arteries - a comparison. *Biorheology*. 1986; 23: 395-433.
- [19] Ookawara S, Ogowa K. Flow properties of Newtonian and non-Newtonian fluid downstream of stenosis. *Journal of Chemical Engineering of Japan*. 2000; 33: 582-590.
- [20] Mahapatra TR, Pal D, Mondal S. Natural convection in a lid-driven square cavity filled with Darcy-Forchheimer porous medium in the presence of thermal radiation. *International Journal of Nonlinear Science*. 2011; 11(3): 366-379.
- [21] Mahapatra TR, Pal D, Mondal S. Influence of thermal radiation on non-Darcian natural convection in a square cavity filled with fluid saturated porous medium of uniform porosity. *Non-Linear Analysis: Modelling and Control*. 2012; 17(2): 223-237.
- [22] Mahapatra TR, Mondal S, Pal D. Heat generation effects in an inclined enclosure under the influence of magnetic field. *ARPJN Journal of Science and Technology*. 2012; 2(6): 556-561.
- [23] Mondal S, Mahapatra TR, Pal D. Natural convection in a two-sided lid-driven inclined porous enclosure with sinusoidal thermal boundary condition. *International Journal of Mechanical Engineering and Technology*. 2012; 33: 187-202.
- [24] Thadakamalla S, Goud BS. Effect of inclined magnetic field on flow, heat and mass transfer of Williamson nanofluid over a stretching sheet. *Case Studies in Thermal Engineering*. 2021; 23: 100819. Available from: doi: 10.1016/j.csite.2020.100819.
- [25] Goud BS, Pramod Kumar P, Malga BS, Reddy YD. FEM to study the radiation, Soret, Dufour numbers effect on heat and mass transfer of magneto-Casson fluid over a vertical permeable plate in the presence of viscous dissipation. *Waves in Random and Complex Media*. 2022. Available from: doi: 10.1080/17455030.2022.2091809.
- [26] Asogwa K, Goud BS. Impact of velocity slip and heat source on tangent hyperbolic nanofluid flow over an electromagnetic surface with Soret effect and variable suction/injection. *Archive Proceedings of the Institution of Mechanical Engineers Part E Journal of Process Mechanical Engineering*. 2022. p. 1989-1996. Available from: doi: 10.1177/09544089221106662.
- [27] Goud BS. Heat generation/absorption influence on steady stretched permeable surface on MHD flow of a micropolar fluid through a porous medium in the presence of variable suction/injection. *International Journal of Thermofluids*. 2020; 7-8: 100044. Available from: doi: 10.1016/j.ijft.2020.100044.